Sublimation of New Matrix Candidates for High Spatial Resolution Imaging Mass Spectrometry of Lipids: Enhanced Information in Both Positive and Negative Polarities after 1,5-Diamin...

ARTICLE *in* ANALYTICAL CHEMISTRY · FEBRUARY 2012

Impact Factor: 5.64 · DOI: 10.1021/ac2033547 · Source: PubMed

4 AUTHORS, INCLUDING:

Aurélien Thomas
University of Lausanne
39 PUBLICATIONS **753** CITATIONS

SEE PROFILE

analytical chemistry

Article

pubs.acs.org/ac

Sublimation of New Matrix Candidates for High Spatial Resolution Imaging Mass Spectrometry of Lipids: Enhanced Information in Both Positive and Negative Polarities after 1,5-Diaminonapthalene Deposition

Aurélien Thomas, Jade Laveaux Charbonneau, Erik Fournaise, and Pierre Chaurand*

Department of Chemistry, University of Montreal, Montreal, Quebec, Canada

Supporting Information

ABSTRACT: Matrix sublimation has demonstrated to be a powerful approach for high-resolution matrix-assisted laser desorption ionization (MALDI) imaging of lipids, providing very homogeneous solvent-free deposition. This work presents a comprehensive study aiming to evaluate current and novel matrix candidates for high spatial resolution MALDI imaging mass spectrometry of lipids from tissue section after deposition by sublimation. For this purpose, 12 matrices including 2,5-dihydroxybenzoic acid (DHB), sinapinic acid (SA), α-cyano-4-hydroxycinnamic acid (CHCA), 2,6-dihydroxyacetphenone (DHA), 2′,4′,6′-trihydroxyacetophenone (THAP), 3-hydroxypicolinic acid (3-HPA), 1,8-bis(dimethylamino)naphthalene (DMAN), 1,8,9-anthracentriol (DIT), 1,5-diaminonapthalene (DAN), *p*-nitroaniline (NIT), 9-aminoacridine (9-AA), and 2-mercaptobenzothiazole (MBT) were investigated for lipid detection efficiency in both positive and negative ionization modes, matrix interferences, and stability under vacuum. For the most relevant matrices, ion maps of the different lipid species were obtained from tissue sections at high spatial resolution and the detected peaks were characterized by matrix-assisted laser desorption ionization time-of-flight/time-of-flight (MALDI-TOF/TOF) mass spectrometry. First proposed for imaging mass spectrometry (IMS) after sublimation, DAN has demonstrated to be of high efficiency providing rich lipid signatures in both positive and negative polarities with high vacuum stability and sub-20 μm resolution capacity. Ion images from adult mouse brain were generated with a 10 μm scanning resolution. Furthermore, ion images from adult mouse brain and whole-body fish tissue sections were also acquired in both polarity modes from the same tissue section at 100 μm spatial resolution. Sublimation of DAN represents an interesting approach to improve information with respect to currently employed matrices providing a deeper analysis of the lipidome by IMS.

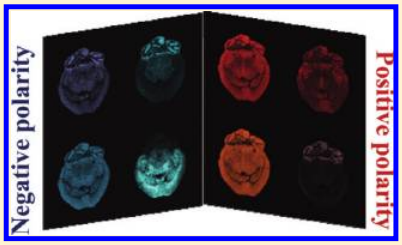

Essential for all living cells, lipids are the most common constituents of biomembranes.[1] Furthermore, they act as regulators for various biological processes such as homeostasis, metabolism, cell adhesion and migration, signal transduction, and apoptosis.[2] These important physiological roles are associated with the numerous diseases in which lipid expression is altered including atherosclerosis, cancer, and Alzheimer's disease.[3−5] Lipidomics, the science aiming to analyze lipids in biological systems, is still considered an emergent field in the "omics cascade".[2] Owing to its complexity, with thousands of dynamic compounds to characterize and monitor, the development of analytical strategies represents a great challenge in which mass spectrometry is considered one of the most powerful tools.[6,7] Regarding this ongoing challenge, imaging mass spectrometry (IMS) is an innovative tool for direct analysis of tissue sections leading to information on the spatial localization of analytes.[8,9] It is now possible to map the evolution of expression profiles of hundreds of potential biomarkers in an unbiased and specific fashion while maintaining a high correlation between the resulting molecular images and the histology of the sections.[10−12] Recently, numerous studies have demonstrated the power of IMS for lipid mapping in brain tissue or the investigation of cancer biopsies.[13] IMS workflow includes different steps going from cutting of fresh frozen tissues (5−20 μm thickness) to section preparation carried out on a sample plate. The entire surface is then rastered according to a user-defined array of fixed dimension and spatial resolution (typically between 10 and 200 μm). At each coordinate, a mass spectrum is acquired. Data is then processed by dedicated software to generate molecular images.[14,15]

In this workflow, homogeneous matrix application constitutes an important issue to ensure high spatial resolution. Different approaches have been developed to form homogeneous matrix crystals across the section and limit lateral migration of the molecules.[16] Among these coating procedures, both manual and automatic systems have been developed.[17] Particularly, automated spray systems and microdroplet inkjet printers are widely used in the IMS laboratory.[18,19] If each system presents some advantages and drawbacks in terms of

Received: December 16, 2011
Accepted: January 13, 2012
Published: January 14, 2012

resolution and reproducibility,[16] a common feature is the use of solvent mixture during matrix application. This aspect introduces an inherent limitation for high-resolution IMS due to risk of delocalization. Recently introduced as a novel approach for matrix application, sublimation has shown to be very powerful for the imaging of low-molecular-weight molecules, particularly phosphoplipids.[20] In their simplest form, sublimation systems consist of a sublimation glassware, a heated bath, and a vacuum pump. Within a few minutes, this process will form an exceptionally homogeneous film of matrix on the section.[21] The most common IMS matrix-assisted laser desorption ionization (MALDI) matrices have been reported for sublimation including 2,5-dihydroxybenzoic acid (DHB) and α-cyano-4-hydroxycinnamic acid (CHCA).[22,23] If these matrices have demonstrated relatively good lipid desorption/ionization efficiencies in positive ion mode, they generate low negative ion yields.[21] The associated loss of information is important since phospholipids, sulfatides, ceramides, cardiolipins, and gangliosides are mainly ionized in the negative mode.[3,24−26]

However, some matrices have been reported for MALDI analysis of lipids in negative mode.[27] As an example, 2,6-dihydroxyacetphenone (DHA) has been largely employed for negative detection of lipids despite its rapid sublimation under vacuum.[26,28] To overcome this issue, the use of aniline to form ionic matrix from DHA has shown to improve stability over 30 min in the high-vacuum environment of MALDI time-of-flight (TOF) mass spectrometers. This delay is still limiting for most IMS applications where a multitude of data points are acquired over longer periods of time.[29] In another example, Sun et al. have demonstrated the use of 9-aminoacridine (9-AA) for phospholipid and cardiolipin analysis in negative ion mode from heart lipid extracts.[30] More recently, an interesting work has been presented by the Caprioli group, investigating buffer washing of the section to improve lipid signals in the negative ionization mode.[31]

Evaluation of novel matrix candidates for sublimation deposition toward high-resolution lipid IMS represents an interesting challenge to improve information beyond that recovered from existing protocols. For this purpose, various MALDI matrices were compared in terms of sublimation ability, sensitivity in both positive and negative ionization modes, matrix cluster interferences, and stability under vacuum. Among investigated candidates, this study revealed a particular interest for 1,5-diaminonapthalene (DAN) after sublimation providing highly informative images of lipids at high spatial resolution. Lipid ion images from mouse brain and from a whole-body fish sections are presented with spatial resolutions from 100 down to 10 μm. Identification of detected lipids was carried out directly from tissue section using MALDI-TOF/TOF mass spectrometry.

MATERIALS AND METHODS

Chemicals and Reagents. Liquid chromatography grade solvents were purchased from Sigma-Aldrich (St. Louis, MO, U.S.A.). DHB, sinapinic acid (SA), CHCA, DHA, 2′,4′,6′-trihydroxyacetophenone (THAP), 3-hydroxypicolinic acid (3-HPA), 1,8-bis(dimethylamino)naphthalene (DMAN), 1,8,9-anthracentriol (DIT), DAN, *p*-nitroaniline (NIT), and 2-mercaptobenzothiazole (MBT) were purchased from Sigma-Aldrich (St. Louis, MO), and 9-AA was from Acros Organics (Morris Plains, NJ).

Phosphatidylinositol (PI) (18:1/18:1), phosphatidylcholine (PC) (14:0/14:0), phosphatidylserine (PS) (14:0/14:0), cardiolipin (CL) (18:1/18:1−18:1/18:1), phosphatidylethanolamine (PE) (18:0/18:0), and phosphatidylglycerol (PG) (18:2:18:2) standards were purchased from Avanti Polar Lipids, Inc. (Alabaster, AL). Stock solutions were prepared at 100 μg/mL in ethanol.

Tissue Sampling, Sectioning, and Coating. Mice (15 days) were euthanized by CO_2 asphyxiation. After sacrifice, dissected organs were flash-frozen by slow immersion in liquid nitrogen to avoid shattering. *Xiphosphorus maculatus* fish was immobilized by immersion in ice water at 4 °C for at least 10 min until cessation of opercular movement to ensure death by hypoxia. Then, flash freezing of the whole-body was achieved as described above. All animal studies were approved by the local Ethical Committee of the University of Montreal.

All tissues were sectioned at 10 μm thickness using a Leica CM3050 cryostat (Leica Microsystems GmbH, Wetzlar, Germany) and thaw-mounted on indium−tin oxide-coated glass slides (Delta Technologies, Stillwater, MN). Sections were dried in a desiccator prior to matrix deposition. Conjointly, serial sections were collected and stained with hematoxylin and eosin (H&E) using standard protocols to assess the histological accuracy of ion images. Direct comparisons between matrices were performed on sections from three different tissue blocks of liver due to the homogeneity encountered in this tissue. DAN matrix removal prior to staining of the fish section was achieved by immersion in 70% ethanol for a few seconds.

Matrix deposition was carried out in a sublimation apparatus (Chemglass Life Science, Vineland, NJ) as previously described.[21] For each matrix, sublimation protocol was optimized for a fixed vacuum of 5×10^{-2} Torr monitoring temperature, time of application, and matrix deposited amounts measured with a high-precision balance to ensure the best MALDI efficiency.

MALDI Mass Spectrometry. Profiling and imaging MS of tissue sections were performed on a MALDI TOF/TOF Ultraflextreme mass spectrometer equipped with SmartBeam II Nd:YAG/355 nm laser operating at 1 kHz and providing a laser focus down to 20 μm in diameter for the "minimum" focus setting (Bruker Daltonics, Billerica, MA). For each matrix, laser fluence was optimized to obtain the best signal-to-noise (S/N) ratio, keeping maximum resolution. These settings also provided for optimal reproducibility. For profiling MS data acquisition, five accumulations of 100 shots were carried out randomly on the tissue sections. For IMS data acquisition, 100 shots were summed per array position. Consecutive positive and negative IMS measurements from a same tissue section were acquired with a spatial resolution of 100 μm after a pixel-shift of 50 μm in both x and y dimensions. High spatial IMS measurements were acquired with a lateral resolution of 10 μm.

Profiling and imaging data acquisitions were performed in reflectron geometry under optimized delayed extraction conditions with a source accelerating voltage of +25 and −20 kV, in a mass range of 640−1040 and 640−1640 Da in positive and negative polarities, respectively. A mass resolution of $M/\Delta M$ 20 000 was typically achieved in the mass window of phospholipids (i.e., 600−1000). External calibration was carried out in quadratic mode using a lipid and peptide mixture to obtain five points of calibration over the mass range. A mass accuracy better than 40 ppm was obtained across a tissue section image.

dx.doi.org/10.1021/ac2033547 | *Anal. Chem.* 2012, 84, 2048−2054

Lipid characterization was performed by comparing accurate mass measurements with the LIPID MAPS prediction tool (http://www.lipidmaps.org/tools/index.html) and confirming by MS/MS in LIFT-TOF/TOF mode. MS and MS/MS data were processed using FlexAnalysis v3.3, and ClinProTools v2.2 softwares (Bruker Daltonics, Billerica, MA). Total ion currents (TIC) were calculated from peaks with a signal-to-noise intensity ≥6. Image data were reconstructed and visualized using Fleximaging v2.1 software (Bruker Daltonics, Billerica, MA).

RESULTS AND DISCUSSION

Evaluation of Novel Matrix Candidates: Potential of DAN for Lipid Imaging. We investigated whether the use of alternative matrix candidates could improve MS spectral qualities in high spatial resolution lipid imaging MS, for both positive and negative ions. Twelve MALDI matrices were investigated including some usually not employed for lipid analysis (i.e., DAN or HAP), as well as others known to have a poor stability under high-vacuum conditions (i.e., DHA or NIT).[23,32,33] For each matrix, sublimation protocols were optimized to obtain the best detection efficiency (Table 1). For that, time and temperature of the process were systematically investigated to achieve optimal solid-to-gas-phase transition resulting in a homogeneous coating on the MALDI plate. To control the sublimation process, the matrix weight by surface unit was also measured. As shown in Table 1, a range going from 50 to 200 $\mu m/cm^2$ was measured according to the matrix, which is in agreement with usually reported values.[20,21] If all of the investigated matrices were able to sublimate, as predicted some of them were not stable in the high-vacuum MALDI source of the TOF instrument ($\sim 10^{-8}$ mbar). Particularly, DHA, NIT, and DMAN quickly sublimated in less than 20 min under these conditions and were eliminated from this study although, for example, NIT presented very intensive lipid signals in positive mode (data not shown).[34] Conversely, other tested matrices did not demonstrate a rapid instability in the MALDI source. Notably, DHB and DAN showed high stability to high MS instrument vacuum with no significant signal alteration observed within an overnight period, a condition necessary for IMS of large-size tissue sections or at high spatial resolution.[21]

Table 1. Potential and Experimental Settings of Investigated Matrices for High Spatial Resolution Imaging of Lipids after Sublimation Deposition[a]

matrix	positive polarity	negative polarity	sublimation temperature (°C)	sublimation time (min)	deposited amount ($\mu g/cm^2$)
CHCA	**	*	180	20	50
DAN	****	****	140	5	110
DHA	–	–	140	2.45	120
DIT	**	**	140	2.5	100
DHB	***	**	140	4.25	120
DMAN	–	–	140	2	150
MBT	****	**	140	3.5	80
NIT	–	–	100	3	110
SA	*	*	165	10	150
THAP	****	**	160	2	180
3-HPA	**	*	160	5	100
9-AA	**	*	190	15	110

[a]The number of stars indicates the observed performance of the matrix according to the polarity with *, **, ***, **** representing low, medium, high, and very high, respectively. Matrices unstable under vacuum are not evaluated (–).

Whereas several matrices including DHB, CHCA, DIT, and HAP can be employed for lipid imaging in positive ionization mode, others such as THAP, MBT, and DAN also produced particularly enriched lipid signatures. Indeed, an overall better sensitivity was observed with DAN when monitoring spectral TIC compared to other coatings (see Supporting Information Figure S-1A). Figure 1 presents two-dimensional (2D) density plots obtained for the comparison of the four most relevant matrices in both ionization modes from liver tissue sections. This data visualization mode presents the advantage of immediate comparison in the same window replicate measurements for several matrices to rapidly find similarities and differences in the lipid pattern (each spot line representing a detected peak according to its abundance scale).[35] In positive ionization mode, the observed lipid species from liver tissue sections were overall the same across the different matrices. A difference was the relative abundance of these according to the m/z range (Figure 1A). DAN and MBT gave a very similar pattern shape with better sensitivity for lower m/z values compared to DHB and THAP. This shift in the pattern results from the formation of potassium and sodium adducts, promoted when DHB or THAP are employed. However, this shift was less pronounced in brain tissue sections probably due to the higher salt concentration in this organ, enhancing adduct formation independently of the matrix used (see Supporting Information Figure S-2).[36]

Conversely, most of investigated matrices were not suitable in the negative ionization mode providing poor sensitivity and a lack of information. However, the use of DAN resulted in a very rich lipid signature comparable in TIC and numbers of observed signals to those observed in positive mode. As demonstrated in the 2D density plot of the Figure 1B, an overall enrichment was achieved with DAN when compared to the negative ionization density plots obtained with DHB, MER, and THAP. This enrichment was associated with a considerable gain in sensitivity over the entire m/z range of interest (see Supporting Information Figure S-1B). DAN's abilities to deprotonate lipids during MALDI ionization are not clear and should require further studies. However, the reductive properties of DAN compared to other investigated matrices could be an explanation of this phenomena.[32] DAN could act as a "proton pump" during the gas-phase ion–molecule reactions following laser desorption, promoting ionization of abundant lipids from tissue section in the negative mode.

In association, we also evaluated whether matrix clusters interfered in both polarities over the m/z range of interest (i.e., between 650 and 1600 Da). Although matrix cluster formation is influenced by different factors among which are laser fluence and salt concentration, and will also differ whether acquisition is performed onto or outside of the tissue section,[37] we found that most of the matrices did not create significant background overlap with lipid species in both ionization modes, excepted SA, for which important matrix cluster were detected (data not shown). Furthermore, DHB also induced matrix clusters in negative mode up to 750 Da, as demonstrated in previous work.[31]

Regarding the investigated matrices during this work, the present results demonstrate the potential of DAN for IMS of lipids, offering the possibility to sequentially image the same tissue section with positive and negative polarities.

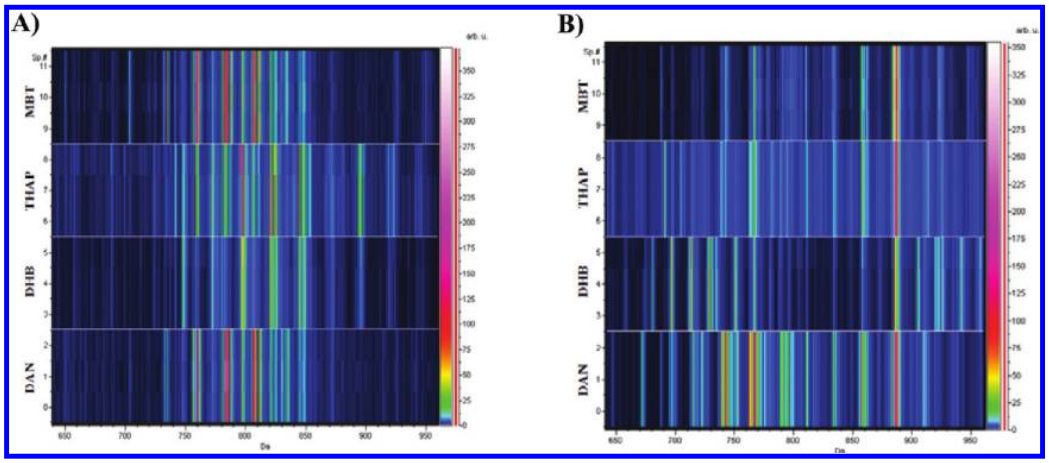

Figure 1. Two-dimensional (2D) density plots in positive (A) and negative (B) polarities for the four most efficient matrices in both modes in the 650−950 Da mass range. For each matrix, blocks were built by three different measurements. For DHB in negative mode, peaks under 750 Da were characterized as matrix clusters.

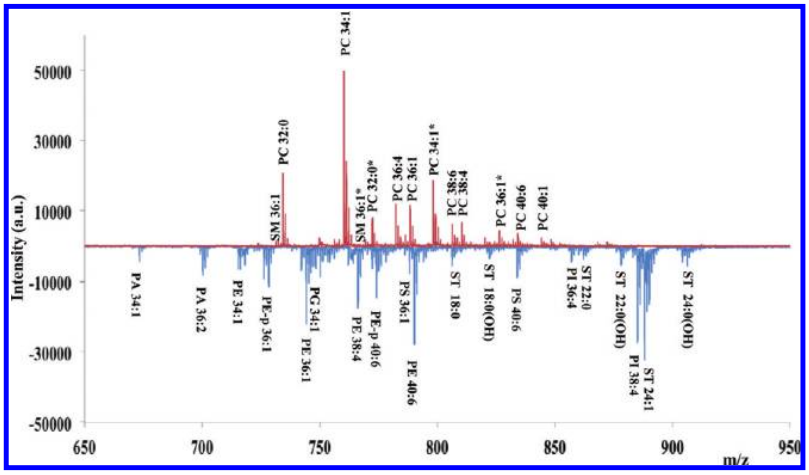

Figure 2. MALDI MS spectra acquired from a mouse brain section coated with DAN by sublimation in the positive (red) and negative (blue) ionization modes. A* indicates potassium adducts.

Characterization of Lipids from Mouse Brain and Liver Tissue Sections. We also investigated whether certain lipid classes were preferentially detected after DAN sublimation with respect to other commonly used matrices. Lipid signals were identified and characterized by MS/MS directly from tissue sections. Figure 2 presents typical positive and negative lipid patterns from a brain tissue section after DAN sublimation. In the positive ionization mode, spectra were mainly constituted by PCs and in a lesser extent by sphingomyelines (SM) species. This characteristic distribution is in agreement with previously published work, independent of the employed matrix.[36,38] As demonstrated in Supporting Information Figure S-3A, MS/MS of *m/z* 782.6 produced a characteristic spectrum corresponding to the PC (16:0/18:2) with characteristic fragment ions at *m/z* 184 and 86 resulting from the polar headgroup ionization.[38]

Investigation of negative ion lipid signature was mainly achieved using DAN owing to the resulting signal enrichment with respect to other matrices (Figure 1). Compared to the positive mode, different species were detected from the tissue sections confirming the importance of this ionization mode for lipid imaging (Figure 2). MS/MS combined with the accurate mass prediction tools allowed us to assign, from both liver and brain tissue sections, different lipid classes of glycerophospholipids including phosphatidic acid (PA), PG, PS, PE, and PI.[13,26] Supporting Information Figure S-3 presents typical MS/MS spectra for several identified phospholipids in negative ionization mode and their proposed fragmentation pathways.

Interestingly, some regiospecificities were observed for certain classes of lipids.[13] For example, the acidic sulfoglycosphingolipids (sulfatides or ST) were abundantly detected in the mouse brain section but not in liver. However, a recent study demonstrated that very small amounts of sulfated lipids were detected from liver extracts, in agreement with our results.[39] As shown in Supporting Information Figure S-4B, the MS/MS spectrum of the ST at *m/z* 906 resulted in specific fragment ions at *m/z* 97 and *m/z* 241 corresponding to the sulfate group and the dehydrated galactose sulfate, respectively.[26] Furthermore, gangliosides GM1 were also detected from brain sections, whereas cardiolipin species were detected from liver sections (Supporting Information Figure S-4).[27,40,41]

Simultaneous Positive and Negative Imaging Mass Spectrometry from a Brain Tissue Section Using 1,5-DAN. As demonstrated in Figure 1, DAN provides rich lipid

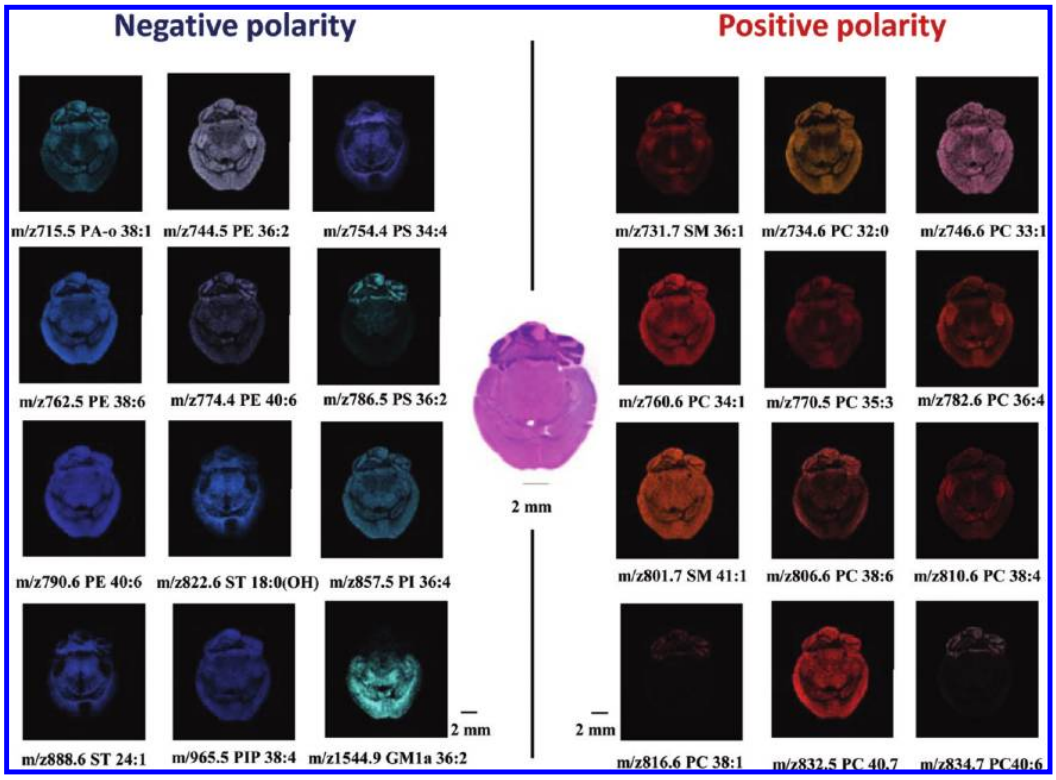

Figure 3. Consecutive IMS of lipids in the negative and positive ionization modes from a transversal mouse brain section after DAN sublimation. Ion images are correlated to a serial section after H&E staining. Imaging MS data were acquired with a lateral resolution of 100 μm with a 50 μm offset between the positive and negative grid arrays.

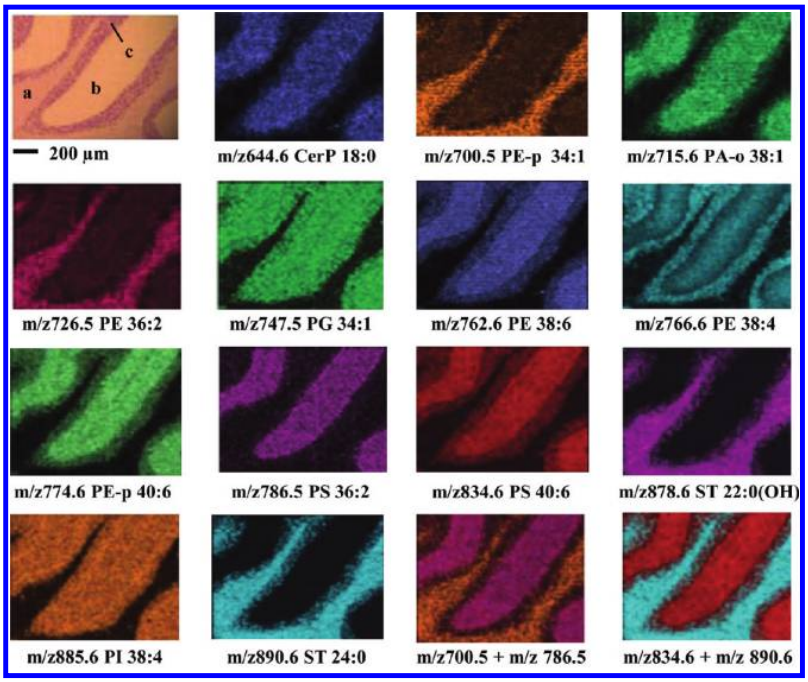

Figure 4. High spatial resolution IMS of lipids in the negative ionization mode from a transversal mouse cerebellum region coated with DAN by sublimation and acquired with a lateral resolution of 10 μm. In the H&E staining, a, b, and c represent white matter and the molecular and granular layers, respectively.

dx.doi.org/10.1021/ac2033547 | *Anal. Chem.* 2012, 84, 2048–2054

signature in both ionization modes compared to other matrices. For this reason, ion images presented in Figure 3 were serially acquired with both positive and negative polarities from the same transversal mouse brain tissue section with a spatial resolution of 100 μm. In this case, the positive grid array was aligned with an offset of 50 μm in both x and y dimensions with respect to the array defined for negative data acquisition. In this case, when using a laser spot diameter of about 40 μm on the target, no ablation overlap was observed (data not shown). Furthermore, no modifications were made for the laser parameter (i.e., laser attenuation offset and focus setting) when switching polarities. As demonstrated in Figure 3, DAN yielded a significant amount of information by serially imaging the same tissue section with positive and negative polarities. Due to the variety of detected species, we observed a better regioselectivity in the negative ion images with respect to positive ones. In this case, the use of DAN provided a larger coverage of the lipidome by IMS. The use of sublimated DAN for lipid IMS may provide additional information for the comprehension of complex mechanistic insights associated to disease or for the discovery of novel biomarkers.

High-Resolution IMS in the Negative Ionization Mode. High-resolution imaging is an interesting approach to analyze with finer details specific tissue regions of interest.[42] To achieve this goal, it is then required to choose a lateral resolution close to or below cellular level (i.e., 10 μm). However, the ability to reach such spatial resolution will depend on several experimental parameters including laser spot size and homogeneity of the matrix deposition without analyte lateral migration.[21,42]

Figure 4 presents high spatial lipid IMS results acquired in the negative ionization mode from a transversal mouse cerebellum coated with DAN by sublimation. Although in this case the laser spot diameter was optimized to be below 20 μm, the oversampling approach was used to compensate for the larger laser spot diameter to reach sub-20 μm resolution. As previously demonstrated, this approach allows us to reduce by a factor of up to 4 the resolution compared to the laser spot size by overlapping each pixel before laser movement.[43] In this way, a lateral resolution of 10 μm was achieved without significant loss of sensitivity and giving an excellent correlation with the H&E staining (Figure 4). Furthermore, the specific brain regions, such as white matter and granular and molecular layers, were univocally detected from the ion images. At this resolution, we demonstrated that some lipids were selectively expressed in certain regions such as white matter for PE-p 34:1 and ST 22:0(OH), whereas CerP 18:0 was only expressed in the molecular layer. Interestingly, the phospholipids PE 38:4 and PS 40:6, for example, were expressed simultaneously in granular and molecular layers but with different intensities allowing the distinction of these two regions. Due to this regioselectivity, composite ion images were generated to reconstitute the cerebellum section anatomy as displayed in Figure 4 (for example, the sum of m/z 700 and 784).

Whole-Body Imaging of a Fish Tissue Section. To illustrate DAN capacity for lipid imaging in different organs, a whole-body *Xiphosphorus maculatus* fish section was serially analyzed in both positive and negative ionization modes with a lateral resolution of 100 μm after an offset of 50 μm in the x and y dimensions as discussed previously (Figure 5). Although not commonly used in IMS, xiphosphorus models are important for melanoma, sex determination, and differentiation, ovoviviparity, and evolution.[44] With a relatively large dimension

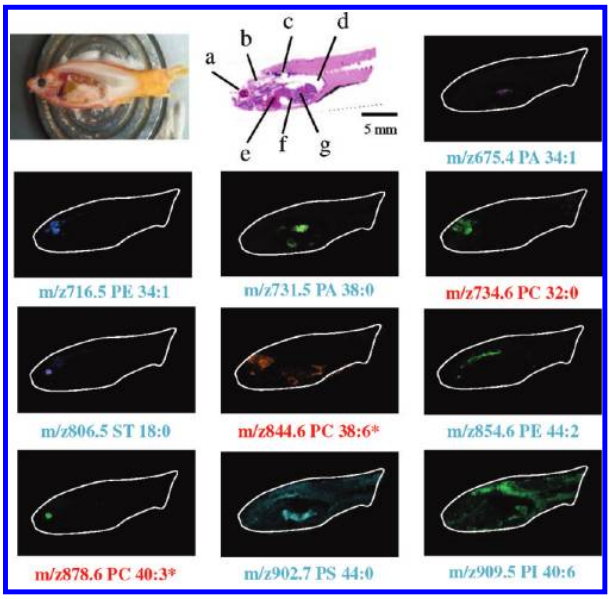

Figure 5. IMS of whole-body fish section in both positive and negative ionization modes after DAN matrix deposition by sublimation. Ion images at different m/z highlight the various organs of the animal. Proposed PCs (in red) are detected in the positive ionization mode and other species (in blue) in the negative ionization mode. a, b, c, d, e, f, and g represent the eye, brain, spinal cord, air bladder, heart, stomach, and gonad, respectively. A $*$ indicates potassium adduct ions.

of 25 mm × 10 mm, successive analysis in both polarities at this resolution corresponding to more than 28 000 pixels leads to a total acquisition time of about 16 h. Such analysis time confirmed DAN stability under high vacuum since no noticeable signal alterations were observed.

Figure 5 presents photomicrographs of the fish mounted on the cryostat block and H&E staining of the analyzed section after matrix removal, as well as several representative ion images of the section. The combination of positive and negative ion IMS results allows us to selectively differentiate most of the visible organs including brain, eye, spinal cord, liver, intestines, and stomach with an excellent correlation with the H&E staining. For example, ST 18:0 and PC 40:3 were predominantly found in the eye, PE 44:2 was exclusively found in the spinal cord, and PC 32:0 was only expressed in the brain. These results were consistent with the enhancement of lipid localization information throughout the body resulting from both positive and negative lipid signatures after DAN sublimation.

CONCLUSIONS

This work presents a comprehensive evaluation of the sublimation potential of current and new matrix candidates for high spatial resolution imaging mass spectrometry of lipids. Among investigated matrices, DAN has demonstrated to be particularly efficient, offering rich lipid signatures in both positive and negative ion polarities associated with low background interferences, high-resolution, and high-vacuum stability. The ability of DAN to enhanced information compared to other matrices, particularly in negative ionization mode, was demonstrated by acquiring positive and negative lipid ion images from the same tissue section as well as high spatial resolution ion images.

dx.doi.org/10.1021/ac2033547 | *Anal. Chem.* 2012, 84, 2048−2054

Monitoring lipid distribution and abundance is of major importance for the understanding of molecular events involved in normal physiological pathways or disease. As demonstrated in this work, DAN sublimation is particular useful to better cover and more deeply analyze the lipidome within tissue sections by high spatial resolution IMS, to help provide meaningful biological and clinical outputs.

■ ASSOCIATED CONTENT

Supporting Information

Additional information as noted in text. This material is available free of charge via the Internet at http://pubs.acs.org.

■ AUTHOR INFORMATION

Corresponding Author

*Phone: (+1) 514-343-2088. Fax: (+1) 514-343-7586. E-mail: pierre.chaurand@umontreal.ca.

Notes

The authors declare no competing financial interest.

■ ACKNOWLEDGMENTS

The authors acknowledge financial support from the Canadian Foundation for Innovation, the Natural Sciences and Engineering Research Council of Canada, and Le Fonds de Recherche du Québec—Nature et Technologies. Dr. A. Thomas is a recipient of a fellowship supported by the Swiss National Science Foundation.

■ REFERENCES

(1) Dowhan, W. *Annu. Rev. Biochem.* **1997**, *66*, 199−232.
(2) Shevchenko, A.; Simons, K. *Nat. Rev. Mol. Cell Biol.* **2010**, *11*, 593−598.
(3) Thomas, A.; Deglon, J.; Lenglet, S.; Mach, F.; Mangin, P.; Wolfender, J. L.; Steffens, S.; Staub, C. *Anal. Chem.* **2010**, *82*, 6687−6694.
(4) Hammad, L. A.; Wu, G.; Saleh, M. M.; Klouckova, I.; Dobrolecki, L. E.; Hickey, R. J.; Schnaper, L.; Novotny, M. V.; Mechref, Y. *Rapid Commun. Mass Spectrom.* **2009**, *23*, 863−876.
(5) Maxfield, F. R.; Tabas, I. *Nature* **2005**, *438*, 612−621.
(6) Thomas, A.; Lenglet, S.; Chaurand, P.; Deglon, J.; Mangin, P.; Mach, F.; Steffens, S.; Wolfender, J. L.; Staub, C. *Thromb. Haemostasis* **2011**, *106*, 20−33.
(7) Palmblad, M.; Tiss, A.; Cramer, R. *Proteomics Clin. Appl.* **2009**, *3*, 6−17.
(8) Chaurand, P.; Schwartz, S. A.; Reyzer, M. L.; Caprioli, R. M. *Toxicol. Pathol.* **2005**, *33*, 92−101.
(9) Ocak, S.; Chaurand, P.; Massion, P. P. *Proc. Am. Thorac. Soc.* **2009**, *6*, 159−170.
(10) Chaurand, P.; Schwartz, S. A.; Billheimer, D.; Xu, B. J.; Crecelius, A.; Caprioli, R. M. *Anal. Chem.* **2004**, *76*, 1145−1155.
(11) Chaurand, P.; Sanders, M. E.; Jensen, R. A.; Caprioli, R. M. *Am. J. Pathol.* **2004**, *165*, 1057−1068.
(12) Franck, J.; Arafah, K.; Elayed, M.; Bonnel, D.; Vergara, D.; Jacquet, A.; Vinatier, D.; Wisztorski, M.; Day, R.; Fournier, I.; Salzet, M. *Mol. Cell. Proteomics* **2009**, *8*, 2023−2033.
(13) Berry, K. A.; Hankin, J. A.; Barkley, R. M.; Spraggins, J. M.; Caprioli, R. M.; Murphy, R. C. *Chem. Rev.* **2011**, *111*, 6491−6512.
(14) Sugiura, Y.; Setou, M. Guide to Planning the Sample Preparation Step. In *Imaging Mass Spectrometry*; Setou, M., Ed.; Springer: Tokyo, Japan, 2010; pp 11−30.
(15) Seeley, E. H.; Oppenheimer, S. R.; Mi, D.; Chaurand, P.; Caprioli, R. M. *J. Am. Soc. Mass Spectrom.* **2008**, *19*, 1069−1077.
(16) Chaurand, P. *Curr. Trends Mass Spectrom.* **2011**, No. July, 30−37.
(17) Chen, Y.; Allegood, J.; Liu, Y.; Wang, E.; Cachon-Gonzalez, B.; Cox, T. M.; Merrill, A. H.; Sullards, M. C. *Anal. Chem.* **2008**, *80*, 2780−2788.
(18) Aerni, H. R.; Cornett, D. S.; Caprioli, R. M. *Anal. Chem.* **2006**, *78*, 827−834.
(19) Chaurand, P.; Norris, J. L.; Cornett, D. S.; Mobley, J. A.; Caprioli, R. M. *J. Proteome Res.* **2006**, *5*, 2889−2900.
(20) Hankin, J. A.; Barkley, R. M.; Murphy, R. C. *J. Am. Soc. Mass Spectrom.* **2007**, *18*, 1646−1652.
(21) Chaurand, P.; Cornett, D. S.; Angel, P. M.; Caprioli, R. M. *Mol. Cell. Proteomics* **2011**, *10*, O110.004259.
(22) Murphy, R. C.; Hankin, J. A.; Barkley, R. M.; Zemski Berry, K. A. *Biochim. Biophys. Acta* **2011**, *1811*, 970−975.
(23) Gustafsson, J. O.; Oehler, M. K.; Ruszkiewicz, A.; McColl, S. R.; Hoffmann, P. *Int. J. Mol. Sci.* **2011**, *12*, 773−794.
(24) Sugiura, Y.; Shimma, S.; Konishi, Y.; Yamada, M. K.; Setou, M. *PLoS One* **2008**, *3*, e3232.
(25) Ivanova, P. T.; Milne, S. B.; Myers, D. S.; Brown, H. A. *Curr. Opin. Chem. Biol.* **2009**, *13*, 526−531.
(26) Jackson, S. N.; Wang, H. Y.; Woods, A. S. *J. Am. Soc. Mass Spectrom.* **2007**, *18*, 17−26.
(27) Wang, H. Y.; Jackson, S. N.; Woods, A. S. *J. Am. Soc. Mass Spectrom.* **2007**, *18*, 567−577.
(28) Woods, A. S.; Jackson, S. N. *AAPS J.* **2006**, *8*, E391−395.
(29) Burnum, K. E.; Cornett, D. S.; Puolitaival, S. M.; Milne, S. B.; Myers, D. S.; Tranguch, S.; Brown, H. A.; Dey, S. K.; Caprioli, R. M. *J. Lipid Res.* **2009**, *50*, 2290−2298.
(30) Sun, G.; Yang, K.; Zhao, Z.; Guan, S.; Han, X.; Gross, R. W. *Anal. Chem.* **2008**, *80*, 7576−7585.
(31) Angel, P. M.; Spraggins, J. M.; Baldwin, H. S.; Caprioli, R. M. *Anal. Chem.* **2011**, in press.
(32) Molin, L.; Seraglia, R.; Dani, F. R.; Moneti, G.; Traldi, P. *Rapid Commun. Mass Spectrom.* **2011**, *25*, 3091−3096.
(33) Shrivas, K.; Hayasaka, T.; Goto-Inoue, N.; Sugiura, Y.; Zaima, N.; Setou, M. *Anal. Chem.* **2010**, *82*, 8800−8806.
(34) Kim, Y.; Shanta, S. R.; Zhou, L. H.; Kim, K. P. *Exp. Mol. Med.* **2010**, *42*, 1−11.
(35) Tsagkrasoulis, D.; Zerefos, P.; Loudos, G.; Vlahou, A.; Baumann, M.; Kossida, S. *BMC Bioinf.* **2009**, *10*, S12.
(36) Delvolve, A. M.; Colsch, B.; Woods, A. S. *Anal. Methods* **2011**, *3*, 1729−1736.
(37) Keller, B. O.; Li, L. *J. Am. Soc. Mass Spectrom.* **2000**, *11*, 88−93.
(38) Sugiura, Y.; Setou, M. *Rapid Commun. Mass Spectrom.* **2009**, *23*, 3269−3278.
(39) Cheng, H.; Sun, G.; Yang, K.; Gross, R. W.; Han, X. *J. Lipid Res.* **2010**, *51*, 1599−1609.
(40) Minkler, P. E.; Hoppel, C. L. *J. Lipid Res.* **2010**, *51*, 856−865.
(41) Whitehead, S. N.; Chan, K. H.; Gangaraju, S.; Slinn, J.; Li, J.; Hou, S. T. *PLoS One* **2011**, *6*, e20808.
(42) Chaurand, P.; Schriver, K. E.; Caprioli, R. M. *J. Mass Spectrom.* **2007**, *42*, 476−489.
(43) Jurchen, J. C.; Rubakhin, S. S.; Sweedler, J. V. *J. Am. Soc. Mass Spectrom.* **2005**, *16*, 1654−1659.
(44) Zhang, Z.; Wang, Y.; Wang, S.; Liu, J.; Warren, W.; Mitreva, M.; Walter, R. B. *PLoS One* **2011**, *6*, e18379.